INTERNATIONAL JOURNAL OF PRECISION ENGINEERING AND MANUFACTURING Vol. 17, No. 7, pp. 857-862 JULY 2016 / 857
DOI: 10.1007/s12541-016-0104-y ISSN 2234-7593 (Print) / ISSN 2005-4602 (Online)

Semi-Active Reaction Force Compensation for a Linear Motor Motion Stage

Duc Canh Nguyen[1] and Hyeong-Joon Ahn[2,#]

1 Department of Mechanical Engineering, Graduate School, Soongsil University, 369 Sangdo-ro, Dongjak-gu, Seoul, 34056, South Korea
2 Department of Mechanical Engineering, Soongsil University, 369 Sangdo-ro, Dongjak-gu, Seoul, 34056, South Korea
Corresponding Author / E-mail: ahj123@ssu.ac.kr, TEL: +82-2-820-0654, FAX: +82-2-820-0668

KEYWORDS: Linear motor motion stage, Residual vibration, Reaction force compensation, Semi-active method

Acceleration and deceleration of a mover excite unwanted vibration to the system base, causing a significant reduction of life and productivity to manufacturing equipment. The system base vibration of a linear motor motion stage can be reduced with a passive reaction force compensation (RFC) mechanism. However, the passive RFC mechanism cannot provide the capability to adjust its stiffness and damping coefficient in real-time. Therefore, resonance may occur if the frequency of the passive RFC mechanism accidentally matches with the frequency components of applied motion profile. This paper presents a semi-active RFC method for a linear motor motion stage using an additional fixed coil. The semi-active RFC mechanism can adjust damping coefficient by changing the resistor load or switching the period of the additional fixed coil. The semi-active RFC mechanism also does not require an additional amplifier or control axis. Mathematical analysis of the semi-active RFC is presented to demonstrate the adjustable damping capability by changing the load resistor. Finally, the effectiveness of the proposed semi-active RFC mechanism is verified via simulations and experiments.

Manuscript received: October 18, 2015 / Revised: March 10, 2016 / Accepted: March 16, 2016

NOMENCLATURE

a-b-c = a-b-c three phase coordinate
a_M = acceleration of the mover
c_{coil} = damping coefficient of fixed coil
c_{MT} = damping of magnet track
F_{coil} = Lorentz force of the fixed coil
F_t = thrust force of the mover
F_{tran} = transmitted force via fixed coil
$I_{a,b,c}$ = three phase currents in a-b-c frame of fixed coil
$I_{ab,bc,ca}$ = currents in resistor loads
$I_{d,q}$ = currents in d-q frame
I_q^{peak} = peak current of fixed coil in q axis
K_{emf} = electromotive force gain
K_f = force constant of fixed coil
k_{MT} = stiffness of magnet track
L_{coil} = inductance of fixed coil
$L_{d,q}$ = inductance of fixed coil in d-q frame
L_q^{load} = inductance of fixed coil in q axis
m_{MT} = mass of the magnet track
m_M = mass of the mover
p = number of pole pairs
R_{load} = load resistance
R_q^{load} = resistor of load in q axis
R_{coil} = resistance of fixed coil
R_q^{coil} = resistor of coil in q axis
V_a^{emf} = electromotive force of fixed coil in q-axis
x_M = position of mover
$\dot{x}_M$ = velocity of mover
x_{MT} = position of magnet track
$\dot{x}_{MT}$ = velocity of magnet track
τ = magnet track pole pitch
ψ = flux linkage of magnet track

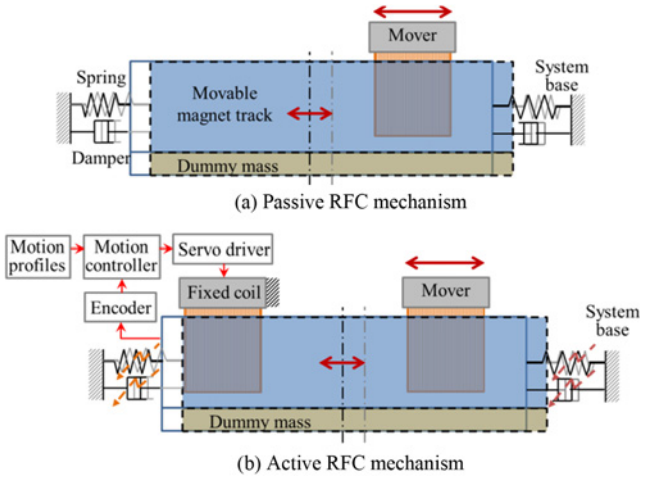

Fig. 1 RFC mechanisms

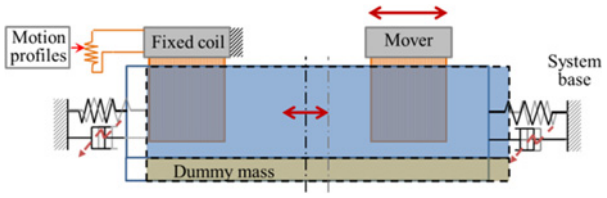

Fig. 2 Semi-active RFC mechanism

Table 1 Comparison of three RFC mechanisms

	Passive	Active	Semi-active
Cost	Cheap (Spring and damper)	Expensive (Control, servo amp. and additional coil)	Cheap (Additional coil)
Energy	No	External energy to drive the coil	Very small energy (for switching)
Adjustable capability	No	Both stiffness and damping	Damping

1. Introduction

Recently, the precision manufacturing industry has been promoting high accuracy and fast response positioning devices, as both moving mass and working area have increased due to improved productivity. In detail, semi-conductor lithography systems necessitate extreme precision and high speed in very long strokes, which have to satisfy 1 nanometer accuracy and 230 wafers per hour over 2 m strokes.[1]

The residual vibration of a system base, due to the high-speed motion of a stage, may reduce both the life and productivity of a manufacturing device.[2] Rapid acceleration or deceleration motions of the stage induce large reaction force on the system base, which causes the system base to oscillate either with considerable amplitude, or for a substantially long time.

A passive RFC mechanism with a movable magnet track, spring and damper can reduce the vibration of the system base.[3-6] The passive RFC mechanism is simple and low cost since the passive RFC mechanism does not require any additional external structures or actuator, as shown in Fig. 1(a). Only a part of the reaction force (the force of the spring and damper) is transmitted into the system base. However, the damping and the spring of the magnet track cannot be adjusted in real-time according to motion profiles.

An active RFC mechanism using an additional coil can optimize its dynamic characteristic by tuning spring and damping of the magnet track, and maintaining a low transmitted force against motion profile variations, as shown in Fig. 1(b).[7] However, the cost and energy consumption of the active RFC mechanism are very high since it needs an additional amplifier as well as a motion control axis.

Linear motor can be used as a variable mechanical damper by changing the external resistance connected to the coil, which is very similar to the concept of semi-active control.[8] The variable damper needs neither servo drive nor motion control axis. Furthermore, the variable damper system does not use any external energy but harvests vibration energy.[9]

In this paper, a semi-active RFC mechanism for a linear motor motion stage using additional fixed coil is proposed. Although the semi-active RFC mechanism does not require additional motion controller axis and servo driver, it can adjust damping by changing the load resistor of the additional fixed coil. Mathematical analysis of the semi-active RFC proves adjustable damping capability by changing the load resistor. Finally, the capability of the semi-active RFC mechanism on the damping adjustment is verified via simulations and experiments.

2. Semi-Active RFC Mechanism

2.1 Principle

The semi-active RFC mechanism consists of a movable magnet track, a fixed coil and a circuit element of impedance adjustment such as variable resistors, as shown in Fig. 2. When the mover moves due to thrust force, its reaction force makes the magnet track oscillate due to the supporting spring and damper, and Lorentz force due to the magnet track oscillation induces electromotive force of the fixed coil. The electromotive force interacts with the magnet track and generates damping force. The electromotive force of the fixed coil can be adjusted by changing its impedance. Therefore, the semi-active RFC mechanism does not need an additional servo driver and motion control axis. In other words, the semi-active RFC mechanism does not use any external energy and can be implemented at very low cost. The three RFC mechanisms are compared in Table 1.

2.2 Mathematical analysis

2.2.1 Circuit equation of the fixed coil

A circuit diagram of a three-phase fixed coil with resistor loads is shown in Fig. 3. The semi-active or fixed coil is wired in star-connection, while the resistor loads are wired in delta-connection.

The three-phase circuits of a fixed coil can be converted into an equivalent circuit in q axis using DQ transformation, as shown in Fig. 4. Here, R_q^{coil} is the resistor of the fixed coil in q axis, L_q^{coil} is the inductance of the fixed coil in q-axis, R_q^{load} is the resistance load of the circuit in q axis and V_q^{emf} is the electromotive force of the fixed coil due to magnet track oscillation.

Resulting circuit equation of the fixed coil can be expressed as Eq.

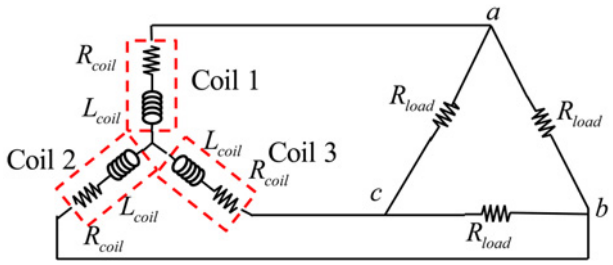

Fig. 3 Circuit diagram of a fixed coil with resistor load

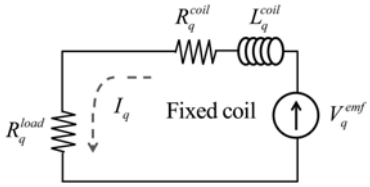

Fig. 4 Equivalent circuit diagram of a fixed coil with resistor load

(1). Here, I_q is the equivalent current in q axis. Since the fixed coil and load resistor are individually wired with star and delta connections, equivalent resistors in q axis should be scaled with $1/\sqrt{3}$ and $1/3\sqrt{3}$, as shown in Eq. (2).[8,10]

$$V_q^{emf} = R_q^{coil} I_q + L_q^{coil} \frac{dI_q}{dt} + R_q^{load} I_q \tag{1}$$

$$R_q^{coil} = \frac{R_{coil}}{\sqrt{3}} \quad \text{and} \quad R_q^{load} = \frac{R_{load}}{3\sqrt{3}} \tag{2}$$

2.2.2 Equation of motion of the magnet track

A schematic diagram in mechanical domain of the semi-active RFC is shown in Fig. 5. The 1-DOF dynamic equation of the magnet track motion is expressed in Eq. (3).

$$m_{MT}\ddot{x}_{MT} + c_{MT}\dot{x}_{MT} + k_{MT}x_{MT} = -F_t + F_{coil} \tag{3}$$

where, m_{MT} is the mass of the magnet track, x_{MT}, $\dot{x}_{MT}$ and $\ddot{x}_{MT}$ are the position, velocity and acceleration of the magnet track, respectively.

Transmitted force to the system base is calculated as Eq. (4)

$$F_{tran} = c_{MT}\dot{x}_{MT} + k_{MT}x_{MT} + F_{coil} \tag{4}$$

2.2.3 Electromechanical system

When the magnet track oscillates due to reaction force, current will be induced in the fixed coil based on Faraday's law. Lorentz force generated by the induced current of the coil and magnetic flux of the magnet track is calculated by Eq. (5).[10]

$$F_{coil} = \frac{3}{2} p \frac{\pi}{\tau} (\psi + (L_d^{coil} - L_d^{coil}) I_d) I_q \tag{5}$$

where, ψ is the flux linkage of magnet track, L_d and L_q are the d-axis and q-axis inductances, p is the number of pole pairs, I_d and I_q are the currents of fixed coil in d and q frame, respectively.

Due to the low inductance of the fixed coil, the Lorentz force of the fixed coil can be approximated as Eq. (6). Here, K_f is motor current gain. In addition, the electromotive force of the fixed coil in q axis can be expressed as Eq. (7). Here, V_q^{emf} is the electromotive force of the fixed coil in q-axis.

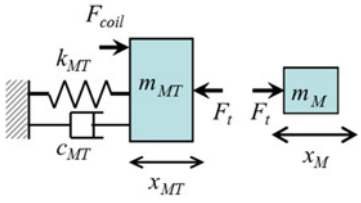

Fig. 5 Schematic diagram of semi-active RFC in mechanical domain

Table 2 Simulation parameters of semi-active RFC

Parameter	Value	Parameter	Value
m_{MT}	21 kg	K_{emf}	20 Vs/m
k_{MT}	195 N/m	R_{coil}	1.5 Ohm
c_{MT}	37 Ns/m	L_{coil}	0.002 H
K_f	20.03 N/A	R_{load}	~
τ	0.048 m	p	2
m_M	7.6 kg		

$$F_{coil} \approx \frac{3}{2} p \frac{\pi}{\tau} \psi I_q = K_f I_q \tag{6}$$

$$V_q^{emf} = K_{emf}\dot{x}_{MT} \tag{7}$$

Using Eqs. (3), (6) and (7), we can derive transfer function from $F_{coil}(s)$ to $sX_{MT}(s)$, as shown in Eq. (8).

$$\frac{F_{coil}(s)}{sX_{MT}(s)} = \frac{K_f K_{emf}}{R_q^{coil} + R_q^{load} + sL_q^{coil}} \tag{8}$$

Considering the low frequency oscillation of the magnet track and the low inductance L_q^{coil}, we can derive an approximate transfer function from the velocity of the magnet track as Eq. (9). The damping coefficient of the fixed coil can be adjusted by changing R_{load}.

$$c_{coil} = \frac{F_{coil}(s)}{sX_{MT}(s)} \approx \frac{K_f K_{emf}}{R_q^{coil} + R_q^{load}} \tag{9}$$

where, c_{coil} is the damping coefficient of the fixed coil.

3. Results of Semi-Active RFC Mechanism

3.1 Simulation parameters

The parameters of the semi-active RFC mechanisms are listed in Table 2 and a picture of the experimental set-up is shown in Fig. 6. Specifications of the linear motor motion stage with semi-active RFC mechanism are as follows: peak force 810 N (continuous 240 N), 1 mm resolution, 380 mm stroke, max 5.0 m/s and max 35 m/s^2 and peak current in the fixed coil 6 A. For the experimental semi-active RFC mechanism, the damping coefficient varies from $c_{coil}^{min} = 0$ ($R_q^{load} = \infty$ Ohm) to $c_{coil}^{max} = 270.7$ Ns/m ($R_q^{load} = 0$ Ohm). The max damping force is calculated with peak current in the coil $F_{coil}^{max} \approx K_f I_q^{peak} = 20.3 \times 6 = 121.8$

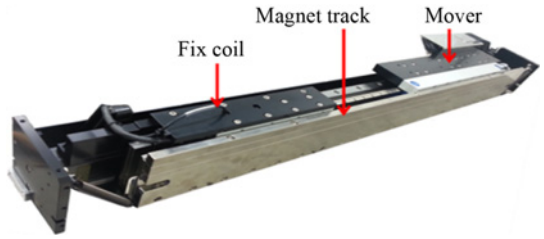

Fig. 6 Experimental set-up for the semi-active RFC mechanism

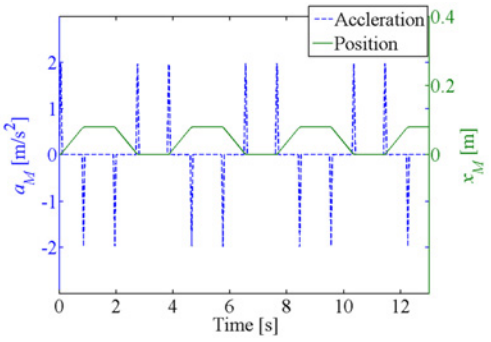

Fig. 7 Motion profile for both simulation and experiment

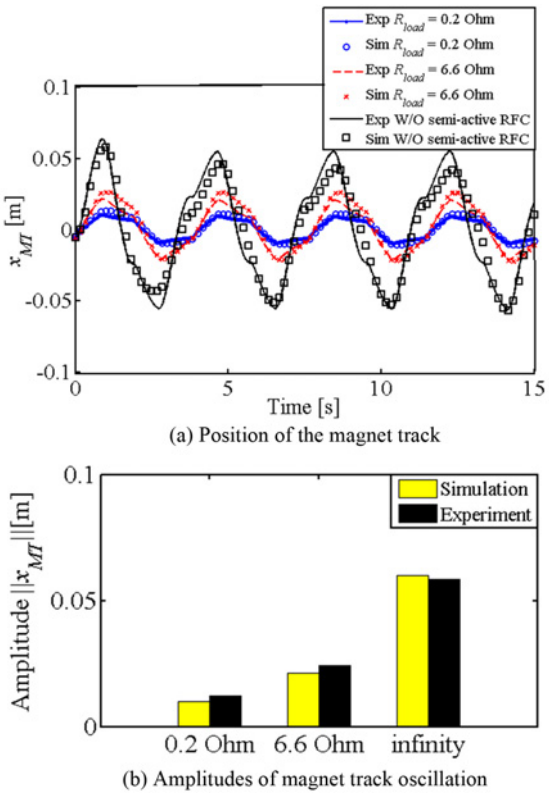

Fig. 8 Magnet track oscillations with various resistor loads

N. Power PMAC is used as a motion controller.[11]

The motion profile used in both the simulation and experiment is long-stroke motion, as shown in Fig. 7.

3.2 Simulation and experimental results

Simulation and experimental results of magnet track motion x_{MT} with R_{load} = 0.2 Ohm, 6.6 Ohm and without the semi-active RFC mechanism (R_{load} = ∞ Ohm), are shown in Fig. 8(a). The solid-lines illustrate the experimental results, while the dash-lines show the simulation results. The amplitude of the magnet track motions in the experimental and simulation results match well with each other, as shown in Fig. 8(b). The amplitude difference of the magnet track motion between experimental and simulation results are 0.0020, 0.0032 and 0.0016 m for 0.2, 6.6 and ∞ Ohm, correspondingly. The discrepancy between the simulation and experiment is expected to come from the asymmetric nonlinear stiffness of the mover cable that is ignored in the simulation. Bigger R_{load} produces smaller damping and larger magnet track motion, which denotes that we can adjust the damping of the magnet track by changing the load resistor. If the load resistance R_{load} is infinity and the damping force of the fixed coil is zero (Eq. (9)) as a consequence, the magnet track has its largest amplitude of oscillation, as shown in the black line of Fig. 8(a). On the other hand, R_{load} = 0.2 or 6.6 Ohm reduces the magnet track oscillation significantly.

In order to confirm the effectiveness of the semi-active RFC mechanism, we indirectly measure the damping force of the fixed coil using two methods. First, the velocity of the magnet track can be calculated from measured magnet track motion using a hall sensor.[12,13] Second, the current I_q can be calculated from measured three-phase currents in *a-b-c* coordinate. In particular, currents I_{ab}, I_{bc} and I_{ca} of resistor loads with star connection are measured using the voltage of the resistor loads. Then, three-phase currents I_a, I_b and I_c are calculated with Eq. (10). Finally, we can calculate I_q and I_d, as shown in Eqs. (11) and (12). The measured currents in *a-b-c* frame and the calculated currents in *d-q* frame with R_{load} = 0.2 Ohm are shown in Fig. 9. Since the magnet track moves in *q* axis, the current in *d* axis is almost zero.

$$I_a = I_{ab} + I_{ac}\,,\quad I_b = I_{ba} + I_{bc}\,,\quad I_c = I_{ca} + I_{cb} \tag{10}$$

$$I_q = \cos\left(\frac{2\pi x_{MT}}{\tau}\right) I_a + \cos\left(\frac{2\pi x_{MT}}{\tau} - \frac{2\pi}{3}\right) I_b + \cos\left(\frac{2\pi x_{MT}}{\tau} + \frac{2\pi}{3}\right) I_c \tag{11}$$

$$I_d = \sin\left(\frac{2\pi x_{MT}}{\tau}\right) I_a + \sin\left(\frac{2\pi x_{MT}}{\tau} - \frac{2\pi}{3}\right) I_b + \sin\left(\frac{2\pi x_{MT}}{\tau} + \frac{2\pi}{3}\right) I_c \tag{12}$$

where, τ is magnet pole pitch of the magnet track.

Fig. 10(a) and (b) show measured damping force of the fixed coil with two resistors R_{load} = 0.2 and 6.6 Ohm, correspondingly. The red-dash lines present the damping force by measured velocity of the magnet track, while black-solid lines illustrate damping force by measured current I_q. The damping force by measured velocity has more fluctuations than that by measured current since the velocity is calculated using the displacement that is measured with a hall encoder of low resolution (100 μm).[12] On the other hand, current is directly measured from voltage of the resistor load.

Transmitted force F_{tran} to the system base and the thrust force F_t due to the mover motion with various resistor loads R_{load} are shown in Fig. 11. Red-dash lines illustrate thrust force calculated with measured current command of the mover coil, while the black-solid lines demonstrate the transmitted force or sum of spring force ($k_{MT}\,x_{MT}$) and damping force ($(c_{MT}+c_{coil})\dot{x}_{MT}$). Transmitted forces to the system base can be reduced

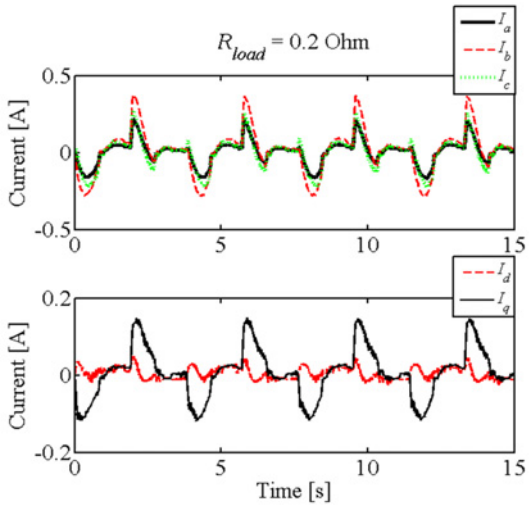

Fig. 9 Coil currents in *a-b-c* and *d-q* frame with R_{load}=0.2 Ohm

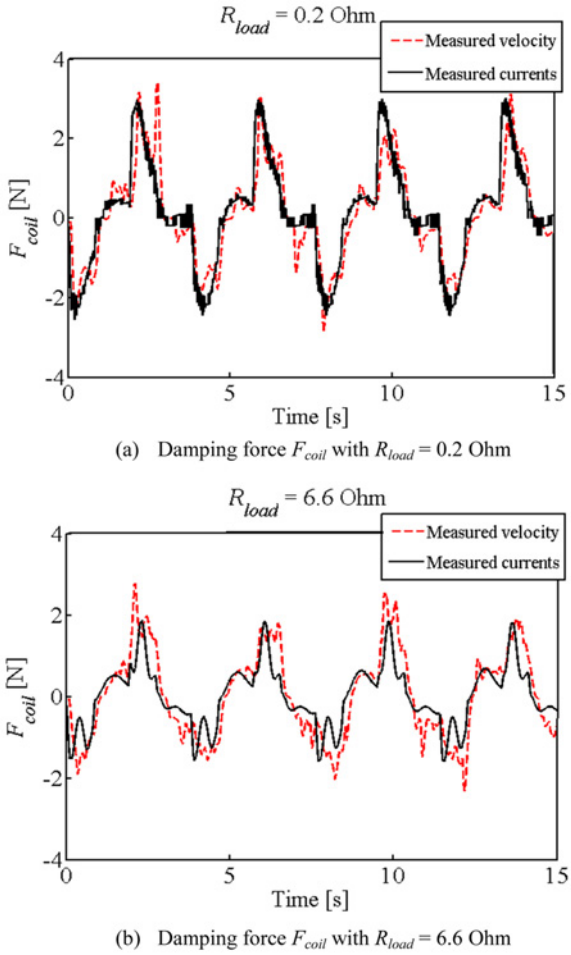

Fig. 10 Damping forces of the fixed coil calculated using velocity and current

significantly (to about 40 % of the thrust force) by adjusting the resistor loads (R_{load} = 0.2 and 6.6 Ohm) of the fixed coil. On the other hand, the transmitted force without resistor load of the fixed coil is almost the same as the thrust force.

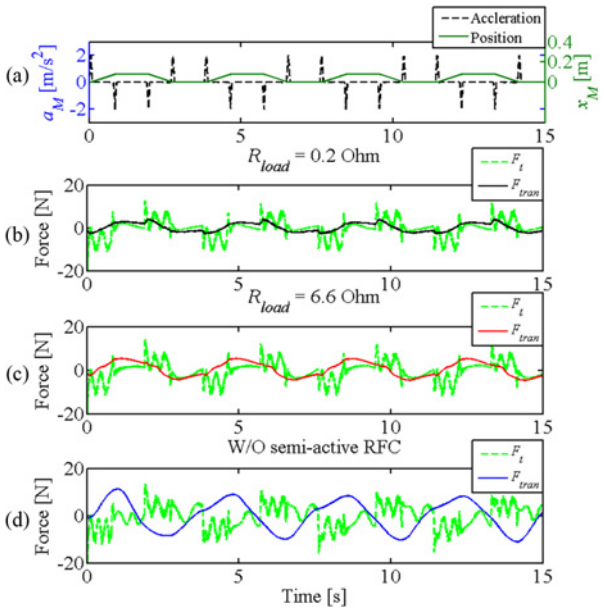

Fig. 11 Force transmissibility of the semi-active RFC system (a) Motion profile of mover motion, (b) R_{load}=0.2 Ohm, (c) R_{load}=6.6 Ohm, (d) without resistor load of the fixed coil

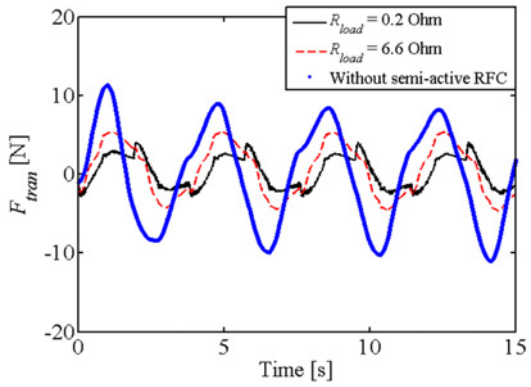

Fig. 12 Measured transmission force with various resistor loads

The transmitted force of the semi-active RFC mechanism with various resistor loads is compared, as shown in Fig. 12. Transmissibility or the ratio of peak transmitted force F_{tran} to peak thrust force F_t is defined in Eq. (13). The transmissibility with various resistors 0.2, 6.6 and infinity Ohm are 15.94%, 24.73% and 48.56% correspondingly. The smaller the load resistance of the fixed coil is, the smaller the transmitted force and the smaller the magnet track motion is.

$$Transmissibility = \frac{|F_{tran}|}{|F_t|} \tag{13}$$

4. Conclusions

We presented a semi-active RFC mechanism for a linear motor

motion stage using an additional fixed coil. This semi-active RFC mechanism does not require any amplifier and control axis, allowing saving to both cost and energy consumption. First, a mathematical model of the fixed coil was derived to obtain the relationship between the damping and resistor load of the fixed coil. Then, the effectiveness of the proposed semi-active RFC mechanism was verified with simulations and experiments.

ACKNOWLEDGEMENT

This work was by Basic Science Research Program through the National Research Foundation of Korea (NRF) funded by the Ministry of Education, Science and Technology (NRF-2013R1A1A2010764).

REFERENCES

1. ASML, “TWINSCAN NXT: 1960Bi,” http://www.asml.com/asml/show.do?lang=EN&ctx=46772&dfp_product_id=7414 (Accessed 19 APR 2016)
2. Tseng, Y.-T. and Liu, J.-H., “High-Speed and Precise Positioning an X-Y Table,” Control Engineering Practice, Vol. 11, No. 4, pp. 357-365, 2003.
3. Cho, K.-J., Choi, D.-S., and Ahn, H.-J., “Mechanism and Control of Reaction Force Compensation of XY Linear Motion Stage System,” Transactions of the Korean Society of Mechanical Engineers A, Vol. 35, No. 6, pp. 599-607, 2011.
4. You, Y.-h. and Ahn, H.-J., “A Passive Reaction Force Compensation (RFC) Mechanism for a Linear Motor Motion Stage,” Int. J. Precis. Eng. Manuf., Vol. 15, No. 5, pp. 797-801, 2014.
5. Nguyen, D. C. and Ahn, H.-J., “Dynamic Analysis and Iterative Design of a Passive Reaction Force Compensation Device for a Linear Motor Motion Stage,” Int. J. Precis. Eng. Manuf., Vol. 15, No. 11, pp. 2367-2373, 2014.
6. Ahn, H.-J., “Eddy Current Damper Type Reaction Force Compensation Mechanism for Linear Motor Motion Stage,” Int. J. Precis. Eng. Manuf.-Green Tech., Vol. 3, No. 1, pp. 67-74, 2016.
7. Nguyen, D. C. and Ahn, H.-J., “A Fuzzy-P Controller of an Active Reaction Force Compensation (RFC) Mechanism for a Linear Motor Motion Stage,” Int. J. Precis. Eng. Manuf., Vol. 16, No. 6, pp. 1067-1074, 2015.
8. Karnopp, D., “Permanent Magnet Linear Motors Used as Variable Mechanical Dampers for Vehicle Suspensions,” Vehicle System Dynamics, Vol. 18, No. 4, pp. 187-200, 1989.
9. Cassidy, I. L., Scruggs, J. T., Behrens, S., and Gavin, H. P., “Design and Experimental Characterization of an Electromagnetic Transducer for Large-Scale Vibratory Energy Harvesting Applications,” Journal of Intelligent Material Systems and Structures, Vol. 22, No. 17, pp. 2009-2024, 2011.
10. Ponomarev, P., “Control of Permanent Magnet Linear Synchronous Motor in Motion Control Applications.” M.Sc. Thesis, Faculty of Technology, Lappeenranta University of Technology, 2009.
11. Delta Tau, “Power PMAC User’s Manual,” 050-PRPMAC-0U0, 2014. ftp://87.245.120.68/support/Hardware/PowerPmac/Users%20Manual/Power%20PMAC%20Users%20Manual.pdf (Accessed 19 APR 2016)
12. Ahn, H. J. and Kim, K. R., “2D Hall Sensor Array for Measuring the Position of a Magnet Matrix,” Int. J. Precis. Eng. Manuf.-Green Tech., Vol. 1, No. 2, pp. 125-129, 2014.
13. Pham, M. N. and Ahn, H.-J., “Horizontal Active Vibration Isolator (HAVI) Using Electromagnetic Planar Actuator (EPA),” Int. J. Precis. Eng. Manuf.-Green Tech., Vol. 2, No. 3, pp. 269-274, 2015.